Bubble Size and Radial Gas Hold-Up Distributions in a Slurry Bubble Column Using Ultrafast Electron Beam X-Ray Tomography

Swapna Rabha, Markus Schubert, Michael Wagner, and Dirk Lucas
Experimental Thermal Fluid Dynamics, Institute of Fluid Dynamics, Helmholtz-Zentrum Dresden-Rossendorf, Dresden 01314, Germany

Uwe Hampel
Experimental Thermal Fluid Dynamics, Institute of Fluid Dynamics, Helmholtz-Zentrum Dresden-Rossendorf, Dresden 01314, Germany

AREVA Endowed Chair of Imaging Techniques in Energy and Process Engineering, Dresden University of Technology, 01062 Dresden, Germany

DOI 10.1002/aic.13920
Published online September 25, 2012 in Wiley Online Library (wileyonlinelibrary.com).

Gas hold-up and bubble size distribution in a slurry bubble column (SBC) were measured using the advanced noninvasive ultrafast electron beam X-ray tomography technique. Experiments have been performed in a cylindrical column ($D_T = 0.07$ m) with air and water as the gas and liquid phase and spherical glass particles ($d_P = 100$ μm) as solids. The effects of solid concentration ($0 \leq C_s \leq 0.36$) and superficial gas velocity ($0.02 \leq U_G \leq 0.05$ m/s) on the flow structure, radial gas hold-up profile and approximate bubble size distribution at different column heights in a SBC were studied. Bubble coalescence regime was observed with addition of solid particles; however, at higher solid concentrations, larger bubble slugs were found to break-up. The approximate bubble size distribution and radial gas hold-up was found to be dependent on U_G and C_s. The average bubble diameter calculated from the approximate bubble size distribution was increasing with increase of U_G. The average gas hold-up was calculated as a function of U_G and agrees satisfactorily with previously published findings. The average gas hold-up was also predicted as a function of C_s and agrees well for low C_s and disagrees for high C_s with findings of previous literature. *AIChE J,* 59: 1709–1722, 2013
Keywords: slurry bubble column, gas hold-up, bubble size distribution, ultrafast electron beam X-ray tomography

Introduction

Slurry bubble column (SBC) reactors find a wide range of application in the chemical process industries. Most important applications of SBC reactors are catalytic hydrogenation of oil, methanol synthesis, Fischer–Tropsch synthesis, and others.[1–3] Particularly, Fischer–Tropsch processes are currently the focus of worldwide academic and industrial interest due to their ability of converting remote natural gas to liquid transportation fuels. The SBC reactor is proven to be the best Reacting device for Fischer–Tropsch processes due to its simple design.[4] The optimal design of SBC reactors for achieving highest levels of conversion requires detailed knowledge on hydrodynamic parameters, such as gas hold-up, phase velocity, bubble size distribution, and mass transfer. Mass transfer in a SBC reactor is mainly controlled by the gas–liquid interfacial area and hence the knowledge of gas hold-up and bubble size distribution is essential. From last decades, extensive research on the effect of presence of solids on the hydrodynamics of SBC reactors is going on, but still the detailed understanding of the underlying flow mechanisms is far from being satisfactory. The role of solids in gas–liquid flows is complex and not fully understood. Presence of solids changes the apparent fluid viscosity and surface tension that might act like surfactants at the gas–liquid interface. With that solid decisively determine macroscopic flow effects and properties, such as bubble formation, bubble rise, gas hold-up, and regime transition, which are in turn key parameters for the heat and mass transfer efficiency in SBC reactors. Few hydrodynamic aspects of SBC reactors have been reviewed by various researchers in the past,[5–8] up to investigations made for elevated temperature and pressure conditions.[8–11] From the previous literature, it was found that slurry viscosity has a strong effect on gas hold-up as compared to pressure and temperature.[12,13,8] This work is related to the hydrodynamic flow behavior in a SBC at ambient conditions and thus studies on SBC at ambient condition are summarized in Table 1 and briefly discussed in the following sections.

Effect of solid concentration (C_s) on gas hold-up

The effect of C_s on gas hold-up in SBC has been studied extensively for instance by Krishna et al.,[17] Vandu et al.,[26] Ruthiya et al.,[27] and Chen et al.[18] They found that an addition of solids essentially increases the pseudoviscosity of the liquid and stabilizes the gas–liquid interface, which in turn

Correspondence concerning this article should be addressed to S. Rabha at s.rabha@hzdr.de.

Table 1. Previous Experimental Studies on SBC at Ambient Conditions

Reference	Experimental Techniques	Gas/Liquid/Solid Properties	Column Dimension/Operating Condition	Parameters Studied
Kim et al.[14]	Bed expansion	Air/water glass beads (d_P = 17–5000 μm)	D_T = 0.186 m, U_G = 0.01 – 0.2 m/s, $C_s \leq 0.20$	• Effect of particle size, concentration on gas hold-up
Jamialahmadi and Mueller-Steinhagen[15]	Bed expansion method	Air/water/styrocel particles (d_P = 0.8–1.3 mm)/nylon particles (d_P = 0.8–2 mm)	D_T = 0.152 cm, $U_G \leq 0.16$ m/s, C_s = 0–0.10	• Effect of solid wettability and concentrations on gas hold-up
Grevskott et al.[16]	CARPT	Air/water/glass beads (d_P = 110–180 μm)	D_T = 0.14, 0.26 m, U_G = 0.02–0.18 m/s, $C_s \geq 0.20$	• Effect of axial solid velocity at different column diameter, gas superficial velocity and solid concentration
Krishna et al.[17]	Pressure sensors	Air/paraffin oil/porous silica particles (d_P = 27–47 μm)	D_T = 0.1, 0.19,0.38 m, $U_G \leq 0.7$ m/s, $C_s \leq 0.36$	• Effect of superficial gas velocity on gas hold-up • Effect of column diameter on gas hold-up
Chen et al.[18]	CARPT	Air/water/solid	D_T = 30.5 cm	• Cross-sectional gas and solid distribution, time averaged particle velocities
Warsito and Fan[19]	ECT	Air/paratherm/polystyrene (d_P = 2 mm)	D_T = 0.10 m, U_G = 0.01 m/s, $C_s \leq 0.10$	• Effect of solid particles on bubble flow structure
Soong et al.[20]	Ultrasound transmission	Nitrogen/water/glass beads (d_P = 10–37 μm)	D_T = 0.889 m, $U_G \leq 0.12$ m/s, $C_s \geq 0.30$	• Effect of gas superficial gas velocity on solid hold-up
Cui and Fan[21]	Laser Doppler Velocimetry	Air/water/acetate particles (d_P = 500 μm)	Rectangular/D_T = 0.102 m, U_G = 0.0025–0.075 m/s, $C_s \leq 0.04$	• Turbulent energy distribution, effect of solid phase on liquid-phase turbulence
Vandu et al.[26]	Gas hold-up measurement and high-speed video camera	Air/paraffin oil/aluminum based catalyst particles (d_P = 10–39 μm)	D_T = 0.1 m, U_G = 0–0.4 m/s, $C_s \leq 0.25$	• Gas hold-up and volumetric mass transfer
Chilekar et al.[22]	Pressure sensors/high-speed video imaging	Air/water/carbon particles (d_P = 40 μm)	D_T = 0.19 m, $0.07 \leq U_G \leq 0.22$ m/s, $0 \leq C_s \leq 0.78$ v/v %	• Average large bubble diameter and compared with the correlation of Krishna et al.[17]
Mena et al.[32]	Bed expansion and static pressure difference	Air/water/calcium alginate beads (d_P = 2.1 mm)	D_T = 0.14 m, $U_G \leq 0.1$ m/s, $0.2 \leq C_s \leq 0.35$	• Effect of presence of solids on regime transition; voidage as a function of gas hold-up
Ruthiya et al.[27]	Pressure time series	Air/water/silica (d_P = 44 μm/ carbon (d_P = 30 μm)	D_T = 0.19 m, $0.045 \leq U_G \leq 0.271$ m/s, C_s = 0.7 v/v %	• Regime transition
Tomiyama[24]	Conductivity probe	Air/water/silica (d_P = 60–150 μm)	D_T = 0.2 m (rectangular), U_G = 0.02,0.034 m/s, $C_s \leq 0.40$.	• Effect of solid concentration on void fraction • Bubble coalescence
Cassanello et al.[25]	CARPT	Air/water/glass beads (d_P = 0.9–5 mm)/ PVC particles (d_P = 5.5 mm)	D_T = 0.10 m, U_G = 0.01–0.11 m/s, C_s = 20–35% of the column height	• Axial mixing time

enhances bubble coalescence and decreases the bubble break-up rate. As a result, reduction in gas hold-up with increasing solids concentration was reported. Krishna et al.[17] studied the influence of silica particle concentration ($0 < C_s < 0.36$) on the total gas hold-up for different gas superficial velocities in two different columns ($D_T = 0.38$ and 0.1 m). The dynamic gas disengagement experiments performed by Krishna et al.[17] show that dense (smaller bubbles) phase gas hold-up significantly reduces with increasing C_s but independent of D_T. However, dilute phase gas hold-up was found to be virtually independent of slurry concentration but significantly dependent on D_T. Further, Vandu et al.[26] found out that due to early creation of large bubbles in the presence of solid particles the transition velocity decreases. On the other hand, several researchers[15,28–32] observed a dual effect of solids on gas hold-up. Kara et al.[28] reported a higher gas hold-up with solids of $d_P = 10$ μm than that with a solids free system. Sada et al.[29] and Bukur et al.[30] also found maximum gas hold-up with C_s, whereas Jamialahmadi and Mueller-Steinhagen[15] demonstrated that an increase or decrease in gas hold-up in an air–water system with the addition of solids depends on the nature of the solids. They found that an addition of nonwettable solids (nylon) reduces gas hold-up, whereas an addition of wettable solids (styrocel) increases gas hold-up. Recently, Mena et al.[32] studied the effect of C_s on the homogeneous–heterogeneous flow regime stability in a $D_T = 0.14$ m column using air, distilled water, and calcium alginate beads ($d_P = 2.1$ mm, $\rho_P = 1023$ kg/m^3). They found that the gas hold-up increases with increasing solids content up to $C_s = 0.03$ and decreases at further addition of solids. They also found that for low C_s (< 0.03) the homogeneous regime was found to be stabilized, whereas for higher C_s (> 0.03) destabilization occurred. From the above discussion, it is found that addition of solid particles to gas–liquid systems may either increase or reduce the bubble coalescence and hence gas hold-up. Furthermore, the reason of this conflicting behavior is not yet explained properly and needs to be investigated.

Effect of solid concentration on bubble size distribution

The bubble size distribution, which provides information about interfacial forces and interaction among the phases, plays an important role in the hydrodynamics and mass-transfer behavior of SBC reactors. However, accurate prediction of the bubble size distribution in SBC reactors is a difficult task. Recently, Chilekar et al.[22] estimated the averaged bubble size in a SBC from pressure fluctuations. Carbon particles of $d_P = 40$ μm were used in both two-dimensional and three-dimensional (3-D) SBCs. The measured average bubble diameters agreed well with the predicted diameters of large bubbles using an empirical correlation of Krishna et al.[17] However, the correlation of Krishna et al.[17] was developed for churn-turbulent gas–liquid flows in a 3-D column. The maximum C_s used by Chilekar et al.[22] was 0.78%, which is not large enough to significantly change the pseudoviscosity of the slurry. Therefore, the effect of solids on averaged bubble diameter is not significant.

Effect of solid concentration on flow structure

The flow structure of the gas phase in a 3-D SBC was first time measured by Warsito and Fan[19] using electrical capacitance tomography (ECT). They studied the effect of polystyrene particles ($d_P = 2$ mm) on the bubble flow structure in an air-paratherm system. They observed bubble break-up with addition of solid particles (5 and 10%). However, due to low spatial resolution of ECT, which is 5–10% of the column diameter and low temporal resolution of max. 100 frames/s, interesting details of the flow, such as bubble size distributions, interfacial area distributions, and gas phase dynamics, could not be resolved.

Empirical correlations for gas hold-up prediction in SBC reactors

Table 2 summarizes the available correlations for predicting gas hold-up in SBC reactors. The effects of U_G and C_s on the gas hold-up are predicted using the available correlations and are shown in Figures 1a&b, respectively. There exists a variation in the predicted trends of the effect of U_G and C_s on gas hold-up. The results of Reilly et al.[33] as well as Sauer and Hempel[34] show a sharp increase of gas hold-up for an increase in U_G, whereas the results of Krishna and Sie[12] and Kara et al.[28] show a gradual increase with U_G (see Figure 1a). Further, the correlations of Kara et al.[28] and Sauer and Hempel[34] show that gas hold-up is almost independent of C_s, whereas Krishna and Sie[12] found a linear decease of gas hold-up with increase in C_s. From these facts, it seems that any correlation to be developed for predicting gas hold-up in SBC reactors accurately has to account for factors like solid properties (d_P, ρ_s, C_s), reactor size (D_T), and gas distribution. To the best of author's knowledge, no correlation is available for bubble size distributions in SBC reactors.

In the above reviewed previous studies on SBC, different flow measurement techniques of varying complexity and principles had been used. They include pressure transducers, local probes, radioactive particle tracking, and tomography methods. Pressure drop measurement together with statistical analysis techniques is a simple and effective method to identify flow regimes, and from the pressure fluctuations, bubble coalescence and breakup are identified in a SBC.[17,27] However, this simple measurement approach is based on the pressure fluctuations measured at the wall and does not reflect the conditions inside the column, which could be different from that at the wall. Local probes, on the other hand, are known to have influence on the flow and fail in piercing small gas bubbles appropriately. Computer automated radioactive particle tracking (CARPT) is a more complex technique, which is based on the tracking of radioactively labeled small particles through the opaque flow. It is well suited for opaque slurries, but unfortunately it does not give information about the phase fraction, though with respect to velocity this technique offers a good spatial resolution (2–5 mm) and temporal resolution (up to 25 Hz).[36,37] Tomographic imaging techniques are also complex but attractive, as the target is the phase fraction distribution. Examples are gamma ray tomography,[38] X-ray tomography,[39] ultrasound tomography,[20,25] and electrical tomography.[19,40] Especially, the latter ECT is considered to be a most powerful technique to study flow dynamics in SBC. However, ECT has serious limitations regarding spatial resolution as discussed earlier. Summarizing, to date, the limitations of existing measurement techniques for highly dynamic and opaque multiphase flows hamper an experimental study of time-resolved flow structures and bubble size distributions, and eventually also gas hold-up in SBC at high superficial gas velocities and higher solid concentrations. Ultrafast electron beam X-ray tomography developed at HZDR is emerging as a powerful technique to capture the real-time data of highly dynamic flows in opaque systems like SBC, because of its high temporal (up to 7000 fps) and spatial resolution ($\sim$1 mm).

Table 2. Correlations for Gas Hold-Up Prediction in SBC at Ambient Conditions

Reference	Gas/Liquid/Solid	Operation Condition	Correlations
Kara et al.[28]	Air/water/coal, dried mineral ash	$U_G = 0.03–0.3$ m/s, $U_{SL} = 0–0.1$ m/s, $C_s = 0–40$ wt %, $D_T = 0.152$ m, $d_P = 10–70$ μm	$\varepsilon_G = \frac{Re_G}{A+BRe_G+CRe_{SL}+D\left(\frac{\varepsilon_S}{\varepsilon_S+\varepsilon_L}\right)}$; A, B, C, and D depends on the particle sizes
Krishna and Sie[12]	Air/paraffin oil, tellus oil/silica	$U_G \leq 0.5$ m s, $C_s \leq 36$ vol %, $D_T = 0.1–0.63$ m, $d_P = 38$ μm	$\varepsilon_G = \varepsilon_{G-large} + \varepsilon_{df}(1-\varepsilon_{G-df})$; $\varepsilon_{G-large} = \frac{U_G - U_{G-df}}{U_{b-large}}$ $U_{b-large} = 0.71\sqrt{gd_B}(SF)(AF)(DF)$ $SF = 1$; $d_B/D_C < 0.125$ $SF = 1.13e^{(-d_B/D_T)}$; $d_B/D_T > 0.6$ $AF = \alpha + \beta(U_G - U_{G-df})$ $DF = \sqrt{1.29/\rho_G}$ $d_B = \gamma(U_G - U_{G-df})^{\delta}$ for Tellus oil, $\alpha = 2.25, \beta = 4.09, \gamma = 0.069, \delta = 0.376$ $U_{G-df} = U_{b-small}\varepsilon_{df}$, $\varepsilon_{df} = \varepsilon_{df,0}\left(\frac{\rho_G}{\rho_{G,ref}}\right)^{0.48}$, $\left(1 - \frac{0.7}{\varepsilon_{df,0}}C_s\right)$, $\varepsilon_{df} = 0.27$ for paraffin oil $U_{b-small} = U_{b-small,0}(1 + \frac{0.8}{U_{b,small,0}}C_s)$, $U_{b-small,0} = 0.095$ m/s
Reilly et al.[33]	Air/water/glass beads	$U_G = 0.02–0.2$ m/s, $C_s \leq 10$ vol %, $D_T = 0.3$ m, $d_P =$ N/A	$\varepsilon_G = 296U_G^{0.44}\ \rho_L^{-0.98}\ \sigma^{-0.16}\ \rho_G^{0.19} + 0.009$
Sauer and Hempel[34]	Air/water/solids ($1020 \leq \rho_P \leq 2780$ kg/m^3	$U_G = 0.01–0.08$ m/s, $C_s = 0–20$ vol %, $D_T = 0.14$ m, $d_P = 2.9$ mm	$\frac{\varepsilon_G}{(1-\varepsilon_G)} = 0.0277\left[\left(\frac{U_G}{(U_G g V_{SL})^{0.25}}\right)^{0.844}\left(\frac{V_{SL}}{Ve_{t-rad}}\right)^{-0.136}\left(\frac{C_s}{C_{s0}}\right)^{0.0392}\right]$
Koide et al.[35]	Nitrogen/water, glycerol, glycol, inorganic electrolytes/ glass and bronze	$U_G = 0.03–0.15$ m/s, $C_s = 0–200$ kg/m^3, $D_T = 0.1–0.3$ m, $d_P =$ N/A	$\frac{\varepsilon_G}{(1-\varepsilon_G)^4} = \frac{A(U_G\mu_L/\sigma g)^{0.918}(g\mu_L^4/\rho_L\sigma^3)^{-0.252}}{1+4.35\left(\frac{C_s}{\rho_P}\right)^{0.748}\left(\frac{\rho_P-\rho_L}{\rho_L}\right)^{0.881}\left(\frac{D_T U_G \rho_L}{\mu_L}\right)^{-0.168}}$; $A = 0.227$ water, glycerol; 0.364 for inorganic electrolytes

In this work, experimental investigations were performed using this X-ray tomography modality to determine the hydrodynamic flow properties in a 3-D SBC. The effect of C_s on gas hold-up, bubble size distribution, and flow structure at different U_G were studied. Essential details of the experimental setup and measurement technique are given in the next section. The results obtained from the tomographic measurements are discussed in the following sections.

Experiments

Experimental setup

The experimental setup consists of a cylindrical column of 70-mm inner diameter and 1500 mm height as shown in Figure 2a. The initial liquid height was adjusted to 1000 mm. The gas distributor used in this study was a perforated plate with uniformly distributed 95 holes of diameter 1 mm as shown in Figure 2a. Air and demineralized water were used as gas and liquid phases, respectively. Spherical glass particles ($d_P = 100$ μm, $\rho_P = 2500$ kg/m^3) were used as solids. All experiments were performed at ambient temperature and pressure conditions. The gas flow rate was controlled by a rotameter. Besides the tomographic scanning plane height (300, 600, and 950 mm above the gas distributor), we varied superficial gas velocities U_G (0.02, 0.036, and 0.05 m/s) and solids concentration C_s (0.05, 0.10, 0.20, and 0.36) in this study.

Ultrafast electron beam X-ray tomography

The ultrafast electron beam X-ray tomography setup is shown in Figure 2b. The tomograph produces slice images from radiographic projections obtained with the scanned electron beam principle. A sharply focused electron beam of up to 10 kW power and 150 kV acceleration voltage is guided and scanned across a circular metal target where X-rays are produced in the beam's focal spot. Rapid deflection by means of an electron optics allows a fast circulation of the focal spot around the SBC. X-rays passing the bubble column are recorded by a very fast multipixel X-ray arc detector coaligned with the target. The tomograph is fast enough to produce up to 7000 cross-sectional images per s at a spatial resolution of about 1 mm.[23,41]

Because of the fast operation of this scanner, the image processing is done offline after the measurements. In this work, the scans were performed at 2500 frames per second (fps) speed for 4 s duration, which gives 10,000 cross-sectional images per single scan. The images are reconstructed from the radiographic projection data with in-house developed reconstruction software. The images have a format of 128 $\times$ 128 pixels whereby each pixel encodes the local linear X-ray attenuation coefficient, which essentially correlates with the local material density. Thus, in the cross-sectional images, the slurry phase and the gas appear with different gray levels. Single particles are too small to be

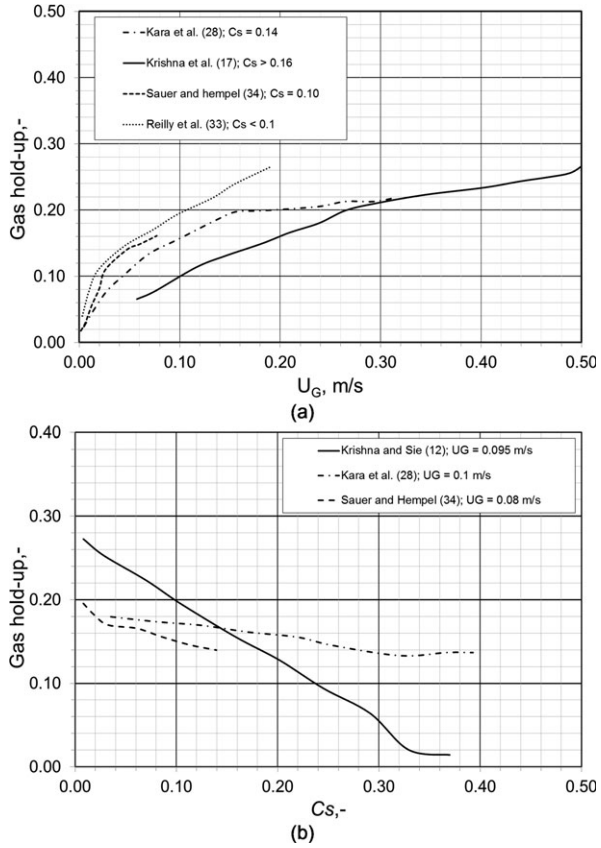

Figure 1. Comparison of gas hold-up as a function of (a) U_G and (b) C_s, estimated using various correlations available in the literature (Sauer and hempel,[34] Kara et al.,[28] Krishna and Sie,[12] Reilly et al.[33]).

resolved (Figure 3). The effective pixel size is 0.55 mm/pixel.

The bubble size distributions in the SBC were approximated from the tomographic images using an algorithm previously developed for wire mesh sensor data.[42] The data were treated as a 3-D volume (series of cross-sectional images over time). First, the data were binarized, and the image volume elements (voxels) were labeled according to the phase they contain. Voxels outside the circular column cross-section were masked out. The distinction between the voxels filled with gas and voxels filled with slurry was made by introducing a threshold. For this study, the threshold has been selected basing on a phantom analysis as 0.47 of the slurry gray value. The sensitivity of the threshold of the reconstructed tomographic images on approximate bubble size distribution was also studied and found that the approximate bubble size distribution was insensitive till ± 5% of the threshold (0.47). The procedure to compute bubble size distribution then has following steps:

- Identification of bubbles, by segmentation of regions of connected gas containing voxels. Each voxel that belongs to one bubble is assigned a unique bubble identification number. Different bubbles receive different bubble identification numbers.
- Calculation of the bubble volume (V_B) by summing the voxels belonging to an identified bubble region

$$V_{B,N} = \Delta x \Delta y \Delta t \cdot w_G \sum_{i,j,k} \varepsilon_{i,j,k} \tag{1}$$

where $\Delta x = \Delta y$ is the in-plane voxel edge length and $\Delta t = 1/f_{sample} = 0.4$ ms the temporal slice separation. To convert the time axis into a length scale, local gas rise velocities would be needed. As they are not available from the data,

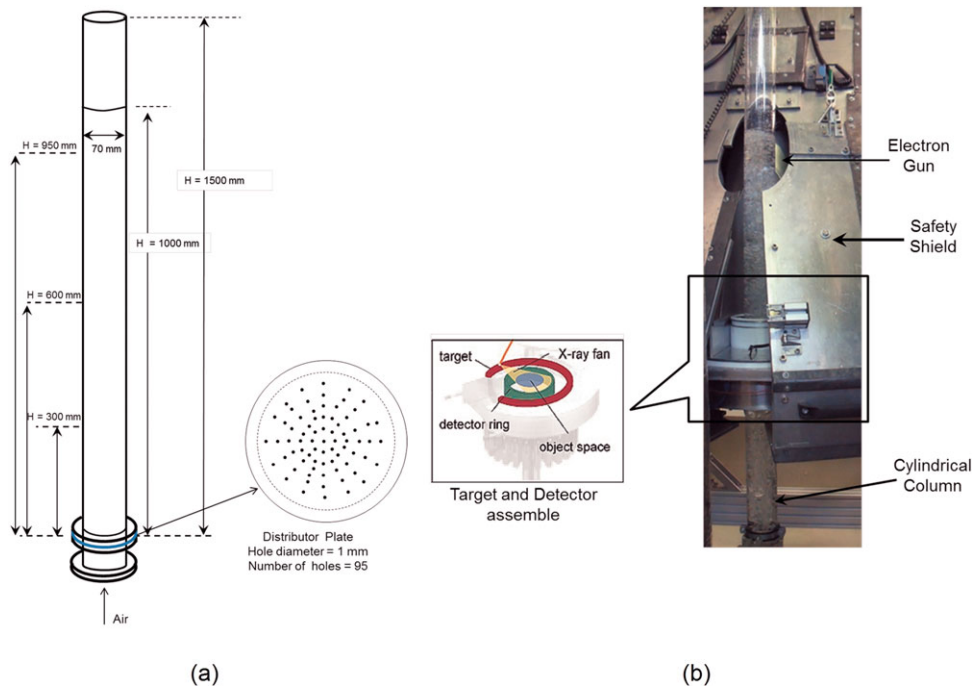

Figure 2. (a) Schematic diagram of the experimental setup and (b) snapshot of the ultrafast electron beam X-ray tomography.

[Color figure can be viewed in the online issue, which is available at wileyonlinelibrary.com.]

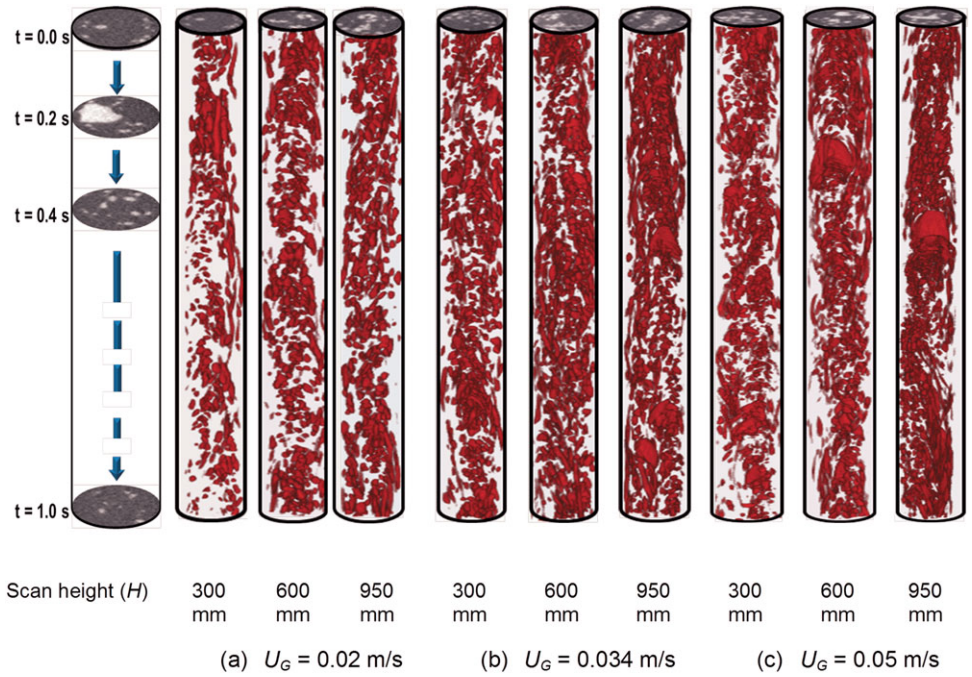

Figure 3. Virtual sectional projection of gas phase distribution in gas-liquid flows at U_G = (a) 0.02 m/s, (b) 0.034 m/s, and (c) 0.05 m/s for three different heights H = 300, 600, and 950 mm.

[Color figure can be viewed in the online issue, which is available at wileyonlinelibrary.com.]

the average gas velocity $w_G = U_G/\varepsilon$ was used in the calculation of the bubble size distribution.

- From the bubble volume equivalent bubble diameters are calculated according to

$$d_{B,n} = \sqrt{\frac{6}{\pi}} \cdot V_{B,N} \tag{2}$$

- Calculation of a statistical distribution with the equivalent bubble diameter as variable. Eventually, the approximate bubble size distribution is represented as local gas hold-up ($\Delta\varepsilon/\Delta d_B$) related to each bubble class width.
- The average bubble diameter is calculated from the approximate bubble size distribution for an individual case as follows

$$d_{B,\text{average}} = \frac{\sum_0^{d_{B,\max}} \left(\frac{\Delta\varepsilon}{\Delta d_B}\right) \cdot d_B}{\sum_0^{d_{B,\max}} \left(\frac{\Delta\varepsilon}{\Delta d_B}\right)} \tag{3}$$

The assumption of all the bubbles moving at average gas velocity ($w_G = U_G/\varepsilon_G$) is a simplified way to estimate approximate bubble size distribution in a bubble column. However, few previous literatures[43,44] suggest that, liquid circulation is negligible in bubble columns with column diameter $D_T < 0.10$ m. In this work, $D_T = 0.07$ m was used for the measurements, and the bubbles were found to be moving upward like a slug flow with negligible liquid circulation. Therefore, the assumption of average gas velocity considered for the calculation of approximate bubble size is not unreasonable. However, it should be also noted that this approximation may not be correct for bubbly flows in large diameter column where the heterogeneous flow regime and liquid circulations are more significant. A detailed description of the bubble size distribution including decomposing of gas fraction distribution according to the bubble classes are given in Prasser et al.[42,45]

Results and Discussion

From the tomography data, we are able to assess the approximate bubble size distribution, the radial gas hold-up profile and the flow structure of the gas phase. The evolving flow structures are being visualized by producing 3-D bubble surface images from a stack of 2500 reconstructed cross-sectional tomographic images captured in 1 s (Figure 3). The vertical coordinate of these virtual projections is the time. The approximate bubble size distribution and radial gas hold-up profiles were calculated for each scan (10,000 images captured in 4 s). The effects of C_s (= 0.05, 0.10, 0.20, 0.36) and U_G (= 0.02, 0.034, and 0.05 m/s) on the flow structure, the approximate bubble size distribution and the radial gas hold-up at different H = 300, 600, and 950 mm were studied and are discussed in the following subsections.

Effect of column height

Figures 3a–c show virtual projections of the gas phase flow structure in a gas–liquid system for H = 300, 600, and 950 mm at U_G = 0.02, 0.034, and 0.05 m/s, respectively. The approximate bubble size distribution at different column heights for U_G = 0.02, 0.034, and 0.05 m/s for the gas-liquid system (C_s = 0) are shown in Figures 4a–c, respectively. The comparison of time-averaged radial gas hold-up profiles at different column heights for U_G = 0.02, 0.034, and 0.05 m/s for the gas–liquid system (C_s = 0) is shown in Figures 5a–c, respectively.

With respect to the axial scan position, insignificant differences were observed for the approximate bubble size distribution and the radial gas hold-up profile at U_G = 0.02 m/s in gas-liquid flow (see Figures 4a and 5a). The approximate bubble size distribution, which represents the local gas hold-up that is related to the bubble class width ($\Delta\varepsilon/\Delta d_B$), was found to be almost homogeneous with a maximum local gas hold-up measured at a bubble size range of d_B = 5–8 mm. The flow

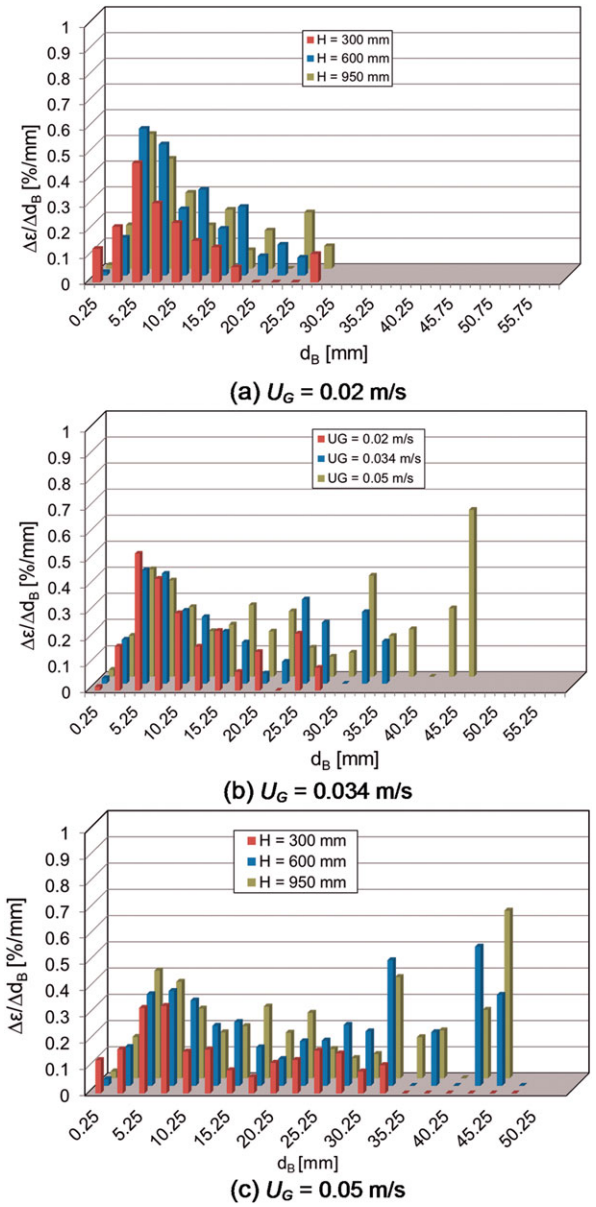

Figure 4. Approximate bubble size distribution of gas–liquid flows at U_G = (a) 0.02 m/s, (b) 0.034 m/s, and (c) 0.05 m/s at three different heights (H = 300, 600, and 950 mm).

[Color figure can be viewed in the online issue, which is available at wileyonlinelibrary.com.]

structure is characterized by a monomodal bubble size distribution at $U_G = 0.02$ m/s for all the scanning planes. A homogeneous bubbly flow can also clearly be identified in the virtual side projections of the gas phase structure for all scanning planes at $U_G = 0.02$ m/s (see Figure 3a).

As U_G increases to 0.034 m/s bubbles start to interact among each other and to coalesce. At $H = 300$ mm, the gas-phase flow structure is characterized by monomodal homogeneous bubbly flow with maximum local gas hold-up at bubble size range $d_B = 5$–10 mm. However, with the flow development (at $H = 600$ and 950 mm) coalescence of the bubbles increases, and the flow structure of the gas phase becomes heterogeneous (Figure 4b). The evolving approximate bubble size distributions of the gas phase at $U_G = 0.034$ m/s are now bimodal size distributions as shown in Figure 4b. The measured bubble size at which maximum local gas hold-up was observed increases with the flow development ($d_B = 5$–10 mm and $d_B = 20$–22 mm at $H = 600$ mm; $d_B = 5$–10 mm and $d_B = 25$–35 mm at $H = 950$ mm). However, the distance from the gas injector was found to be insignificant with respect to the radial gas hold-up profile at $U_G = 0.034$ m/s as shown in Figure 5b. At higher $U_G = 0.05$ m/s, the transition of heterogeneous bubbly flow (at $H = 300$ mm) into churn-turbulent bubbly flow (at $H = 600$ and 950 mm) was observed as shown in Figure 3c. Bimodal bubble size distributions were observed for all the scanning planes (shown in Figure 4c). However, large bubble slugs with an equivalent bubble diameter of $d_B = 32$–42 mm were

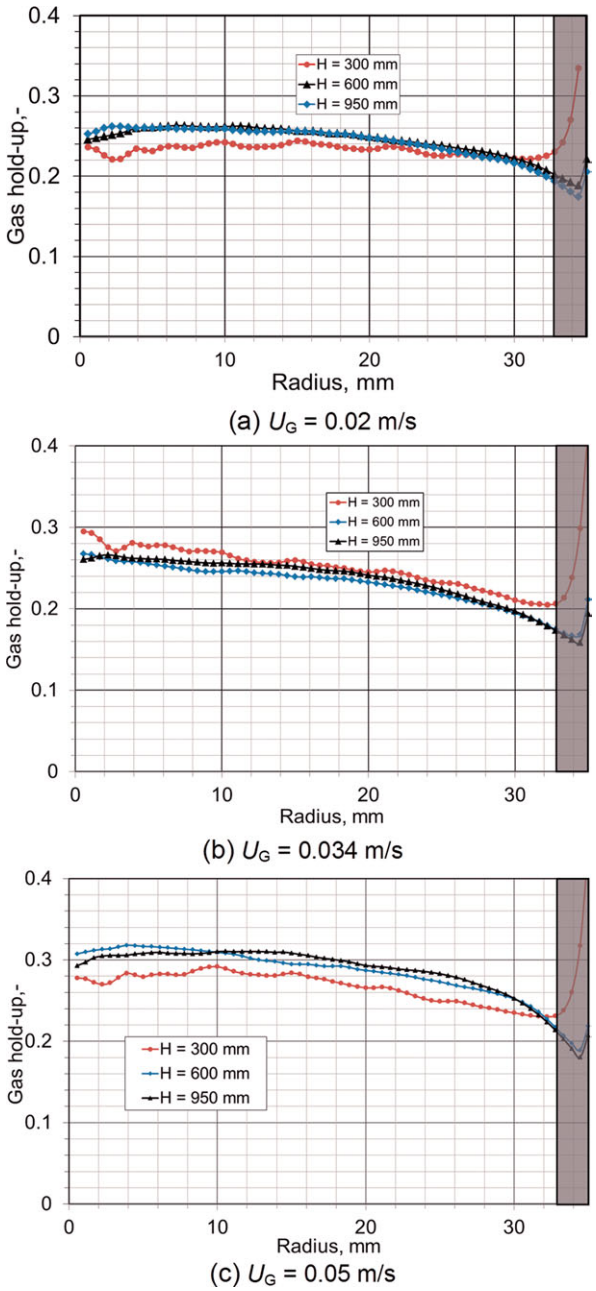

Figure 5. Radial gas hold-up of gas–liquid flows at U_G = (a) 0.02 m/s, (b) 0.034 m/s, and (c) 0.05 m/s at three different heights (H = 300, 600, and 950 mm).

[Color figure can be viewed in the online issue, which is available at wileyonlinelibrary.com.]

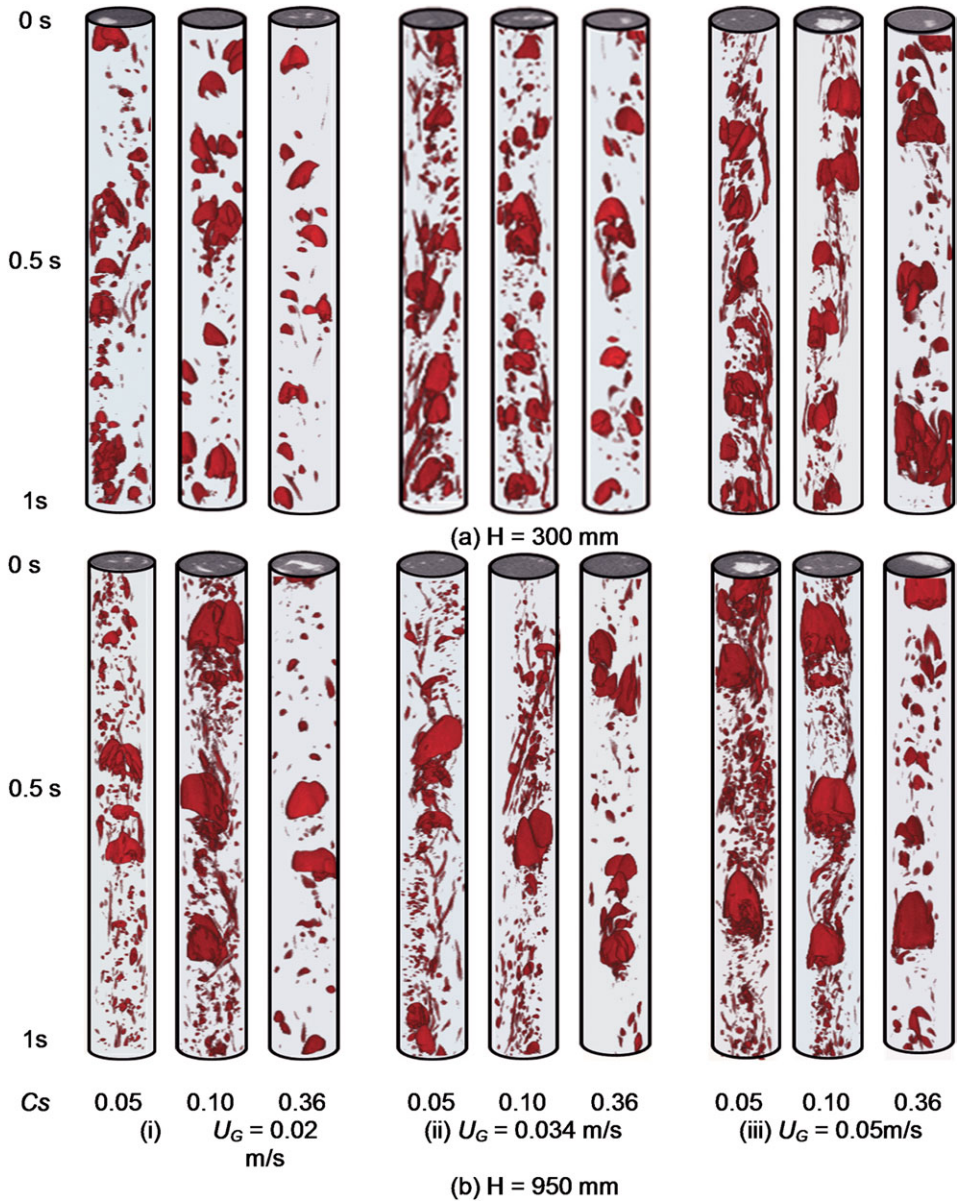

Figure 6. Virtual projection of the gas phase structure in gas-slurry flows at U_G = 0.02, 0.034, and 0.05 m/s for C_s = 0.05, 0.10, and 0.36 at (a) H = 300 mm and (b) H = 950 mm.

[Color figure can be viewed in the online issue, which is available at wileyonlinelibrary.com.]

observed at higher column heights due to bubble coalescence. Similar to $U_G = 0.034$ m/s, the averaged radial gas hold-up profile at $U_G = 0.05$ m/s does not show any significant dependency on the height as shown in Figure 5c.

From the above discussion, it follows that approximate bubble size distributions and as a consequence the flow structure of the gas phase changes as the flow develops in the column. However, the radial gas hold-up of the cross-section remains almost the same throughout the column for the solid-free gas–liquid system. An artificially high value of gas fraction near the wall was observed mainly at column height of $H = 300$ mm. The probable artifacts for the dark region within 2 mm of the wall may be due to a little division of the measurement scan at $H = 300$ mm from the reference scan. The measurements near 2 mm of the wall region were considered to be suspicious at $H = 300$ mm and were not considered for all the measurement cases reported in the article. In the article, the values near the wall region (radial distance = 33–35 mm) were shaded.

Effect of solid concentration

To study the effect of C_s on the gas phase flow behavior in a SBC, experiments have been performed at different C_s ($0 \leq C_s \leq 0.36$) for $U_G = 0.02$, 0.034, and 0.05 m/s. Figures 6a and b shows the virtual projections of gas phase flow structure for different C_s ($0 \leq C_s \leq 0.36$) at $U_G = 0.02$, 0.034 and 0.05 m/s at $H = 300$ and 950 mm, respectively. The effect of C_s on approximate bubble size distributions of the gas phase for different $U_G = 0.02$, 0.034, and 0.05 m/s at $H = 300$ and 950 mm are shown in Figures 7 and 9, respectively. The time-averaged radial gas hold-up at different C_s for $U_G = 0.02$, 0,034, and 0.05 m/s at $H = 300$ and 950 mm are shown in Figures 8 and 10, respectively.

From Figure 6a, it was found that bubbles start coalescing even at low C_s. This behavior can be explained by the fact that the pseudoviscosity of the slurry increases with the addition of solids, which enhanced the coalescence of bubbles and as a result large bubble slugs were formed. In Figure 6a, the

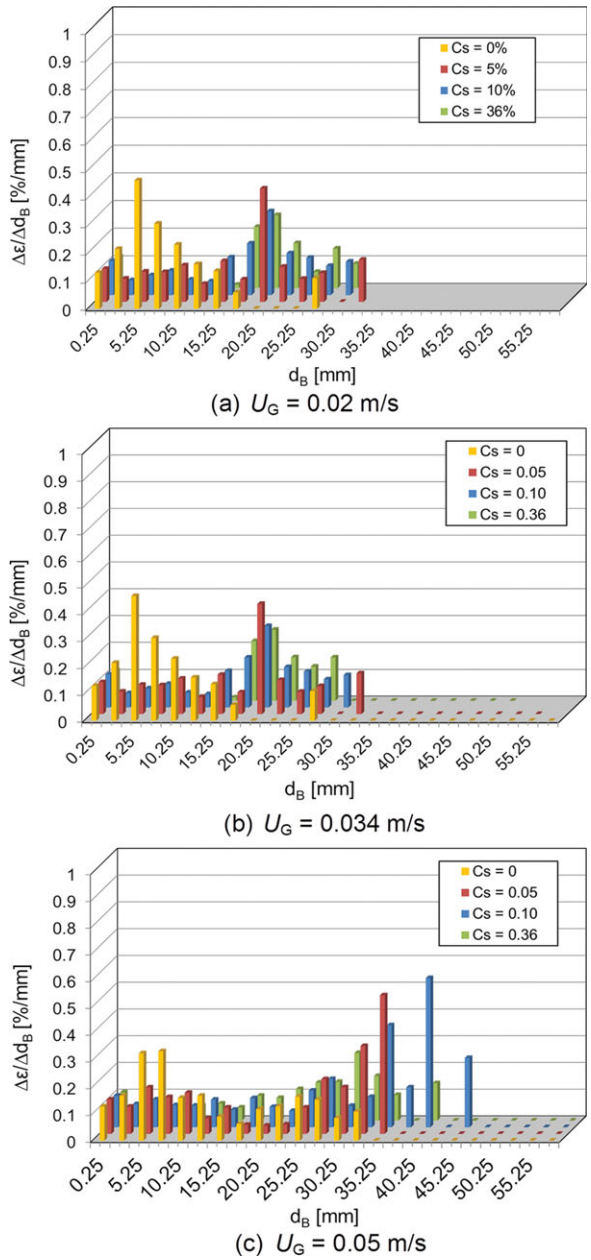

Figure 7. Approximate bubble size distribution in the SBC at U_G = (a) 0.02 m/s, (b) 0.034 m/s, and (c) 0.05 m/s for $0 \leq C_s \leq 0.36$ at H = 300 mm.

[Color figure can be viewed in the online issue, which is available at wileyonlinelibrary.com.]

large bubble slugs were found to concentrate in the center region of the column up to $C_s = 0.10$ at $U_G = 0.02$ m/s. However, at $C_s = 0.36$ large slugs start breaking-up and reduction in the bubble sizes was observed due to the effect of the wall and bubble-particle interactions (Figure 6a(i)). This phenomenon agrees with the observations of Michelsen and Østergaard[46] and Warsito and Fan.[19] The formation of large bubble slugs with the addition of solid particles can also be found in the approximate bubble size distributions at $U_G = 0.02$ m/s at $H = 300$ mm (Figure 7a). The maximum local gas hold-up for gas-liquid flow was found to be within $d_B = 5$–8 mm (Figure 3a), whereas with addition of C_s the maximum local gas hold-up was found to be around $d_B = 20$–25 mm at both $C_s = 0.05$, 0.10, and 0.36. Due to the formation of large bubble slugs with increasing C_s at a constant U_G, the gas momentum per unit mass of slurry decreases, which in turn decreases the total gas hold-up.[17,24] Therefore, due to the coalescence of bubbles and formation of large bubble slugs, the gas hold-up profile at $U_G = 0.02$ m/s and $H = 300$ mm was found to decrease with increasing C_s (Figure 8a).

At $U_G = 0.034$ m/s, the heterogeneous bubbly flow regime for solid-free flow was found to changed into the bubble coalescence regime with increasing C_s (Figure 6a(ii)). The bubble coalescence was found to start early and more significantly compared to $U_G = 0.02$ m/s (see Figure 6a(ii)). Large bubble slugs of equivalent diameter $d_B \sim 32$–35 mm were found at $C_s = 0.05$ and 0.10 (Figure 7b). After attaining a maximum size of the bubble slugs at $C_s = 0.10$,

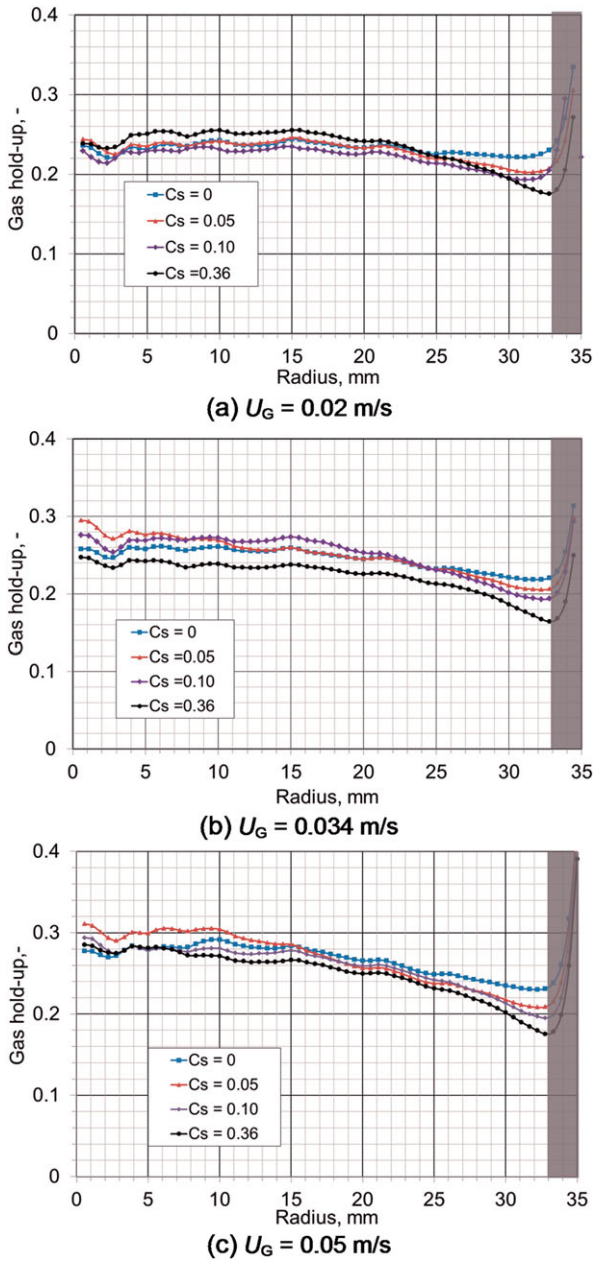

Figure 8. Radial gas hold-up in the SBC at U_G = (a) 0.02 m/s, (b) 0.034 m/s, and (c) 0.05 m/s for $0 \leq C_s \leq 0.36$ at H = 300 mm.

[Color figure can be viewed in the online issue, which is available at wileyonlinelibrary.com.]

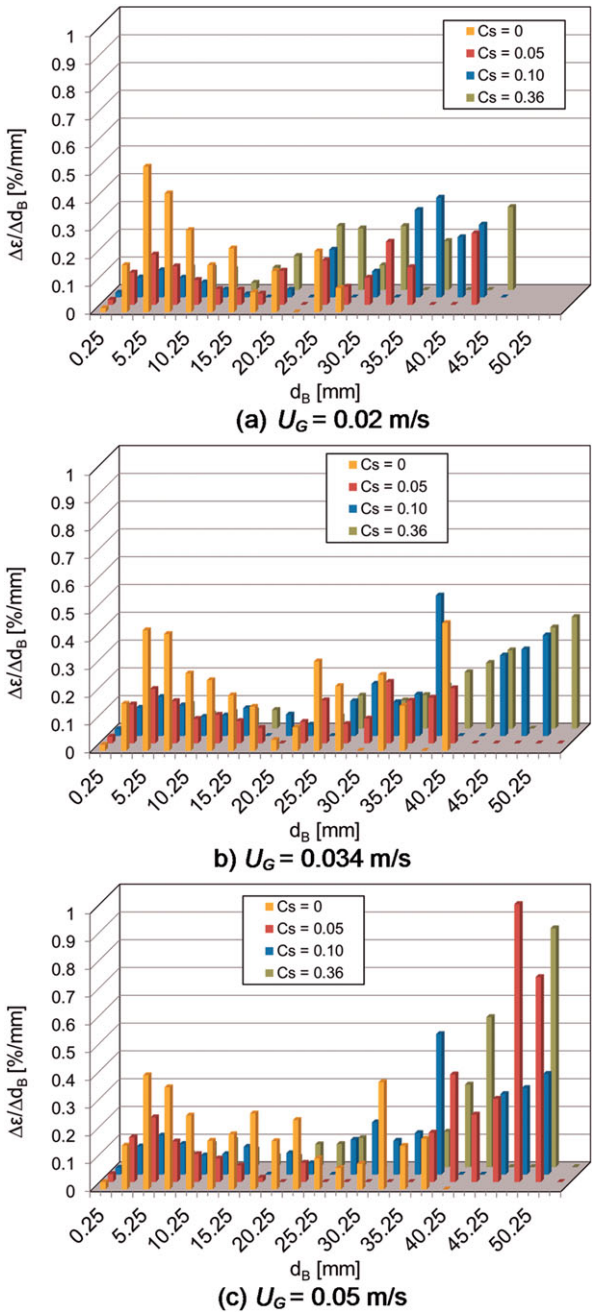

Figure 9. Approximate bubble size distribution in the SBC at U_G = (a) 0.02 m/s, (b) 0.034 m/s, and (c) 0.05 m/s for $0 \leq C_s \leq 0.36$ at H = 950 mm.

[Color figure can be viewed in the online issue, which is available at wileyonlinelibrary.com.]

bubbles start breaking-up after further addition of solids (C_s = 0.36) as shown in Figure 6a(ii). The bubble break-up and reduction of the bubble sizes can also be observed in the approximate bubble size distribution profiles (see Figure 7b). The local gas hold-up was found maximum at d_B = 27.5 mm (C_s = 0.36) as compared to that at d_B = 32–35 mm for C_s = 0.05 and 0.10. Again, the gas hold-up in the cross-section was found to reduce for increasing C_s as shown in Figure 8b. Similar behavior was also found at U_G = 0.05 m/s, where the churn-turbulent flows at C_s = 0 converted to flows with large slugs after addition of solid particles, which affects the approximate bubble size distribution and radial gas hold-up (as shown in Figures 7c and 8c).

The effects of C_s on the flow structure at H = 950 mm are shown in Figure 6b. After addition of solids, bubbles starts to coalesce even at low C_s and low U_G (Figure 6b(i)). Bubble coalescence and formation of large bubble slugs was found to be more significant at a higher column height H = 950 mm as compared to that at H = 300 mm. Figure 9 also shows the presence of large bubble slugs after addition of solid particles (e.g., $d_B \sim$ 32.75, 52, and 52 mm at C_s = 0.05 for U_G = 0.02, 0.034, and 0.05 m/s, respectively). The bubble break-up regime was more prominent with further increase in C_s at H = 950 as compared to that at H = 300 mm (Figures 6a,b). Due to bubble coalescence at low C_s (= 0.05), the radial gas hold-up was reduced, whereas at

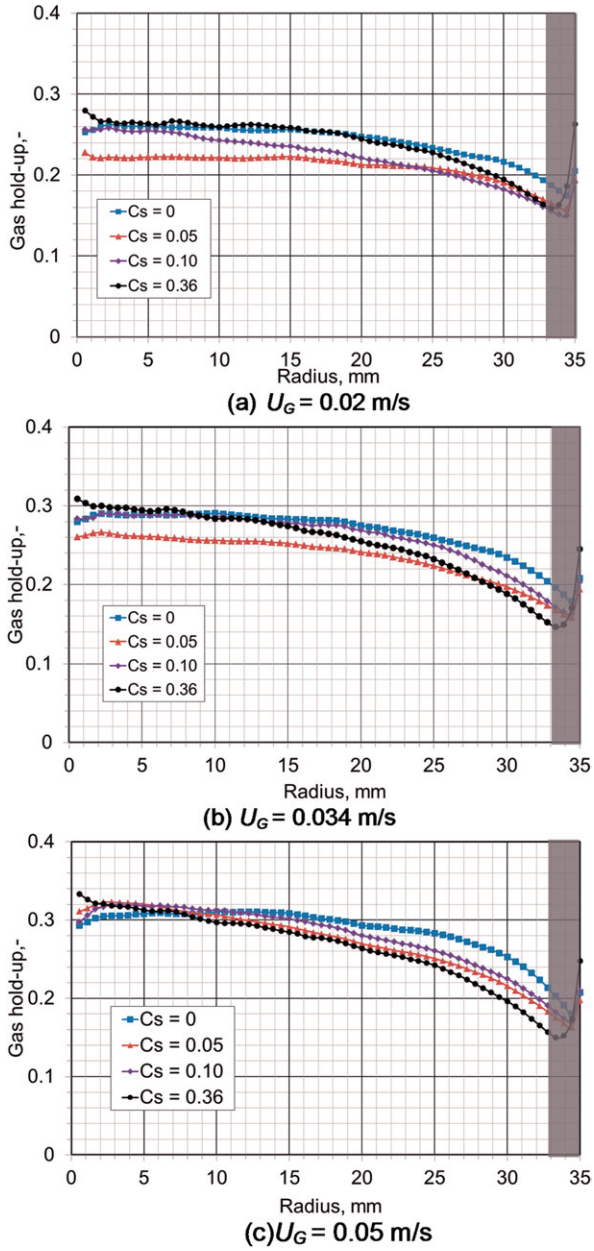

Figure 10. Radial gas hold-up in the SBC at U_G = (a) 0.02 m/s, (b) 0.034 m/s, and (c) 0.05 m/s for $0 \leq C_s \leq 0.36$ at H = 950 mm.

[Color figure can be viewed in the online issue, which is available at wileyonlinelibrary.com.]

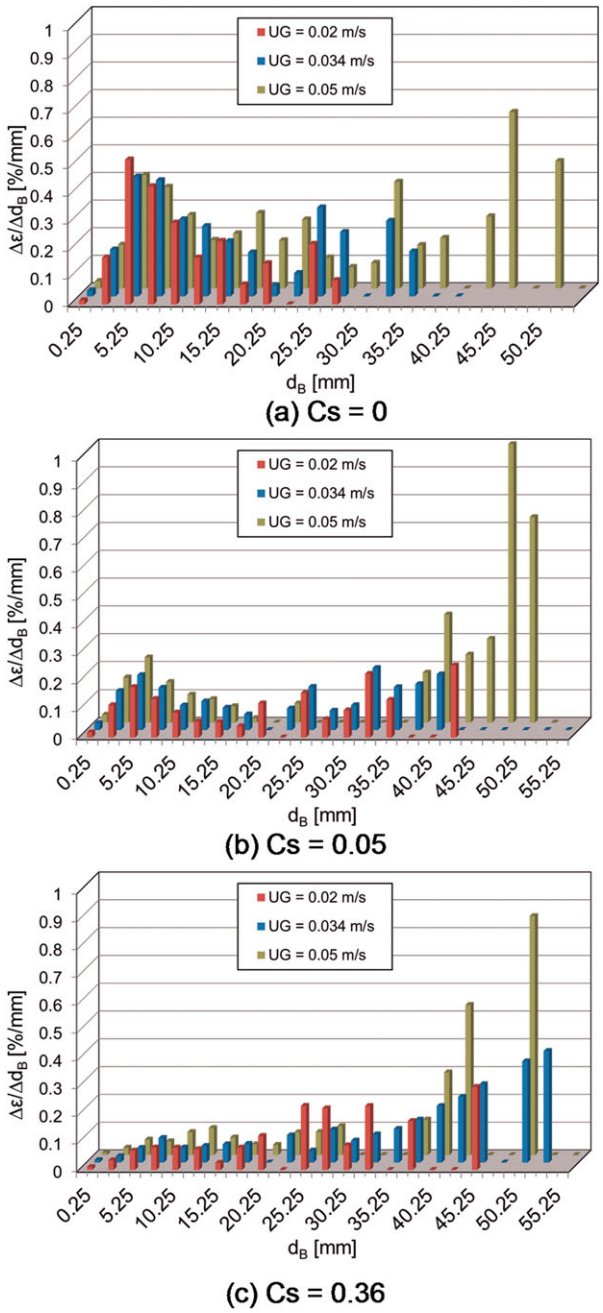

Figure 11. Approximate bubble size distribution in the SBC at C_s = (a) 0, (b) 0.05, and (c) 0.36 for U_G = 0.02, 0.034, and 0.05 m/s at H = 950 mm.

[Color figure can be viewed in the online issue, which is available at wileyonlinelibrary.com.]

higher C_s ($\geq$ 0.10) the radial gas hold-up was found to have increased due to presence of smaller bubbles generated by bubble break-up as shown in Figure 10.

From the study of the effect of C_s on the flow structure, approximate bubble size distribution and radial gas hold-up, it was found that the bubbles start coalescing after addition of solid particles; however, with addition of more solid particles, the bubble break-up regimes start to dominate. This bubble break-up regime phenomenon can be explained by the increased bubble-particle interactions and reduction of available space for the gas-liquid mixture in the presence of solids. It was also found that the transition point between the bubble coalescence and break-up regimes starts decreasing with the increase of superficial gas velocity. This interesting dual effect of solid concentration on gas hold-up was also reported in previous literature.[28,30,32]

Effect of superficial gas velocity

The effects of U_G on the hydrodynamic flow behavior of the gas phase in a SBC for $0 \leq C_s \leq 0.36$ at three column heights were studied. The comparison of approximate bubble size distribution at C_s = 0, 0.05, and 0.36 for different U_G ($0.02 \leq U_G \leq 0.05$ m/s) at H = 950 mm is shown in Figures 11a–c respectively. The effects of U_G on the averaged radial gas hold-up in a SBC at C_s = 0, 0.05, and 0.36 are shown in Figures 12a–c, respectively.

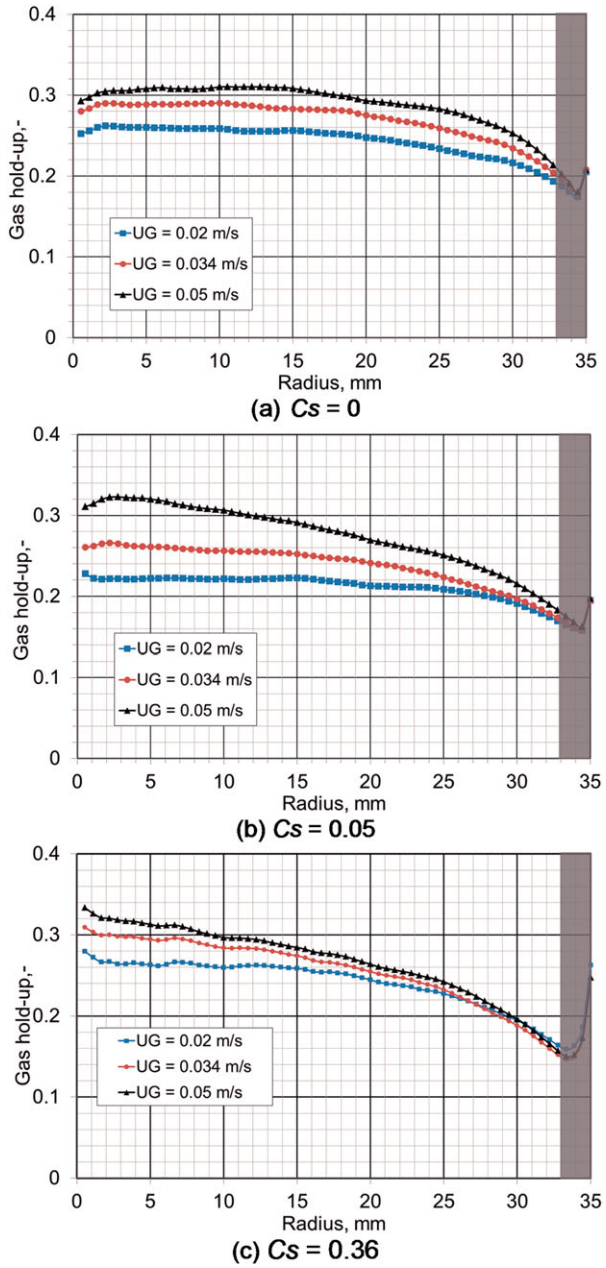

Figure 12. Radial gas hold-up in the SBC at C_s = (a) 0, (b) 0.05, and (c) 0.36 for U_G = 0.02, 0.034, and 0.05 m/s at H = 950 mm.

[Color figure can be viewed in the online issue, which is available at wileyonlinelibrary.com.]

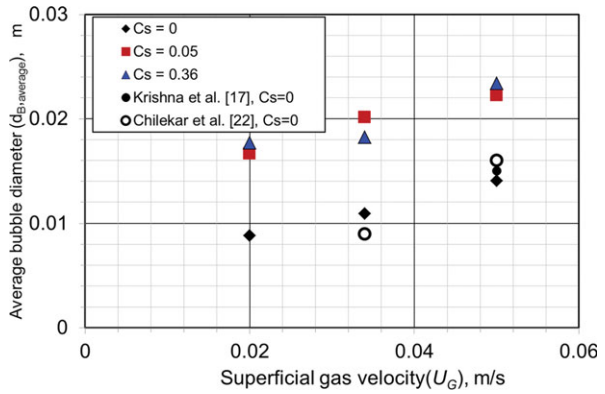

Figure 13. Calculated averaged bubble diameter ($d_{B,average}$) as a function of U_G at H = 300 mm.

[Color figure can be viewed in the online issue, which is available at wileyonlinelibrary.com.]

At $C_s = 0$, homogeneous bubbly flow was observed at low $U_G = 0.02$ m/s. As U_G increases more bubbles were observed and the transition from homogeneous to heterogeneous ($U_G = 0.034$ m/s) and to churn-turbulent bubbly flow ($U_G = 0.05$ m/s) was observed at $H = 950$ mm (see Figure 3). The regime transition at $C_s = 0$ can also be seen from the approximate bubble size distribution profile in Figure 11a. As expected, with the increase of U_G, the total radial gas hold-up at $C_s = 0$ increased, as shown in Figure 12a. The observation could be explained by the fact that with increasing U_G, more bubbles were generated and interaction among the bubbles becomes significant, which increases the overall gas hold-up. As mentioned in the earlier sections, large bubble slugs of equivalent diameter almost equal to the column diameter were observed with the increase in C_s for all the three superficial gas velocity. The increase of the size of bubble slugs with increase of U_G for $C_s = 0.05$ can clearly be seen in the approximate bubble size distribution profile (shown in Figure 11b). The radial gas hold-up at $C_s = 0.05$ (shown in Figure 12b) was found to increase with increasing U_G. However, for very dense systems ($C_s = 0.36$) and in churn-turbulent flow regimes, the increase of U_G has only a slight effect on the averaged radial gas hold-up, as shown in the Figure 12c. A similar observation was also reported in the previous literature.[14,17] From the above observation of the effect of U_G on the radial gas hold-up, it was found that the cross-sectional gas hold-up in SBC increases with U_G at all the solid concentrations ($0 \leq C_s \leq 0.36$) considered in this study.

From the above discussions on the effect of C_s on approximate bubble size distribution at different U_G and H, it was found that the average bubble diameter is significantly higher after addition of solid particles than in the case of a solid-free gas–liquid system ($C_s = 0$). The average bubble diameter (calculated using Eq. 3) as a function of U_G for different C_s is plotted in Figure 13. The average bubble diameter increases with U_G and is found to be in good agreement with the average bubble diameter found by Krishna et al.[17] and Chilekar et al.[22] for a solid free gas–liquid system. The time-averaged gas hold-up over the entire cross-section was also calculated and plotted as a function of U_G in Figure 14. A linear increase of gas hold-up with the increase of U_G was observed at all C_s which agrees with the observation of the previous literature.[15,17,28,32–34] However, the reduction of the average gas hold-up with C_s was found to be less at higher C_s ($C_s = 0.10$ and 0.36) as compared to that at $C_s = 0.05$, which disagrees with the previous literature.[15,17,28,32,34] However, in all the above mentioned previous studies, low-density solids and larger column diameters (see Tables 1 and 2) were used.

Conclusions

The effects of C_s on the flow behavior in a SBC at different U_G were investigated experimentally using ultrafast electron beam X-ray tomography as a noninvasive high-resolution imaging modality. The radial gas hold-up and approximate bubble size distribution as well as the flow structure were extracted from tomographic images, which were captured at 2500 fps for 4 s at different column heights. The flow properties were studied at different U_G

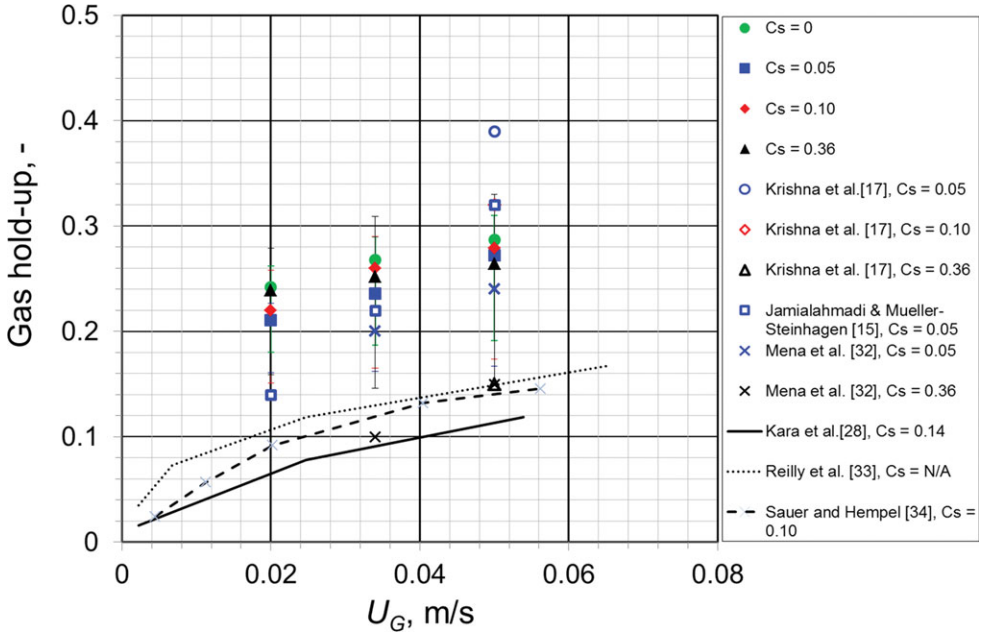

Figure 14. Averaged gas hold-up as a function of U_G at H = 300 mm.

[Color figure can be viewed in the online issue, which is available at wileyonlinelibrary.com.]

($0.02 \leq U_G \leq 0.05$ m/s) and C_s ($0 \leq C_s \leq 0.36$). The key conclusions of this work are the following:

- Ultrafast electron beam X-ray tomography is applicable for the measurement of phase distribution in a three-phase SBC and gives many new insights into the gas phase distribution and its dynamics.
- As U_G increases, transitions from homogeneous to heterogeneous and eventually churn-turbulent regime were observed in gas–liquid flows. The effect of flow development on approximate bubble size distribution is negligible at lower U_G (homogeneous bubble flow); however, at higher U_G, bubble size distribution becomes bimodal as the flow develops. The effect of flow development on the radial gas hold-up was found to be insignificant.
- The cross-sectional gas hold-up was reduced with the addition of solid particles because of the enhanced bubble coalescence. But for high solids concentration large bubbles start breaking-up and radial gas hold-up starts to increase.
- The approximate bubble size distribution in a SBC at higher C_s (> 0.01) was for the first time measured and found to depend on U_G and C_s.
- The average bubble diameter increases with U_G and is found to be in good agreement with the average bubble diameter found by Krishna et al.[17] and Chilekar et al.[22] at solid free gas–liquid system.
- A linear increase of gas hold-up with the increase of U_G was observed at all solid concentrations, which agrees with the observations of the previous literature. However, the reduction of the average gas hold-up with solid concentration was found to be less at higher solid concentrations (C_s = 0.10 and 0.36) as compared to that at C_s = 0.05, which disagrees with findings from the previous literature.

The observed dual effect of the presence of solids on the bubble size distribution and on the radial gas hold-up qualitatively justified the observation of Ruzicka et al.[47] It shows that lower viscosity stabilizes the uniform bubbly flow, whereas higher viscosity destabilizes the bubbly flow. A further systematic study with smaller increments of solids concentration may be helpful to determine the critical solid concentration for the bubble coalescence and breakup regime. Moreover, this work was done in a smaller diameter column where boundary effects are not negligible and slug flow can develop. It will be also interesting to study the effect of presence of solids in large diameter column, where liquid circulation and turbulence are dominating, in the future.

Notation

C_s = solids concentration
d = diameter, mm
D_T = column diameter, mm
f = frequency, Hz
H = column height at which scan is positioned, mm
Re = Reynolds number
t = time, s
U = superficial velocity, m/s
V = volume of bubble, mm^3
w = Average velocity, m/s
x = distance in horizontal direction, mm
y = distance in vertical direction, mm

Greek letters

ε = gas hold up
ρ = density, kg/m^3
σ = surface tension, N m

Subscripts

B = bubble
df = dense phase
G = gas phase
H = hole
P = solid particle
L = liquid phase

Literature Cited

1. Shah YT. *Gas–Liquid–Solid Reactor Design*. New York: McGraw-Hill, 1979.
2. Ellenberger J, Krishna R. A unified approach to the scale-up of gas–solid fluidized bed and gas–liquid bubble column reactors. *Chem Eng Sci*. 1994;49:5391–5411.
3. De Swart JWA, Krishna R. Effect of particles concentration on the hydrodynamics of bubble column slurry reactors. *Chem Eng Res. Des Trans Ind Chem Eng*. 1995;73:308–313.
4. Krishna R. A scale-up strategy for a commercial scale bubble column slurry reactor for Fischer–Tropsch synthesis. *Oil Gas Sci Technol—Rev IFP*. 2000;55(4):359–393.
5. Pandit, AB, Joshi, JB. Mass and heat transfer characteristic of three phase sparged reactors. *Chem Eng Res Des*. 1986;64:125–157.
6. Yang GQ, Bing D, Fan, LS. Bubble formation and dynamics in gas–liquid–solid fluidization: a review. *Chem Eng Sci*. 2007;62:2–27.
7. Guillen DP, Daniel SW, Steven PA, Michael ZP. Review of experimental capabilities and hydrodynamic data for validation of CFD based predictions for slurry bubble column reactors. In: AIChE Meeting, Salt Lake City, UT, 2007.
8. Behkish A, Lemoine R, Sehabiague L, Oukaci R, Morsi BI. Gas holdup and bubble size behaviour in a large-scale slurry bubble column reactor operating with an organic liquid under elevated pressure and temperature. *Chem Eng Sci*. 2007;128:69–84.
9. Deckwer WD, Louisi Y, Zaidi A, Ralek M. Hydrodynamic properties of the Fischer–Tropsch slurry process. *Ind Eng Chem Proc Des Dev*. 1980;19:699–708.
10. Pohorecki R, Moniuk W, Zdrojkowski A. Hydrodynamics of a bubble column under elevated pressure. *Chem Eng Sci*. 1999;54(21): 5187–5193.
11. van der Schaaf J, Chilekar VP, van Omman JR, Kuster BFM, Tinge JT, Schouten JC. Effect of particle lyophobicity in slurry bubble columns at elevated pressures. *Chem Eng Sci*. 2007;62:5533–5537.
12. Krishna R, Sie ST. Design and scale-up of the Fischer–Tropsch bubble column slurry reactor. *Fuel Process Technol*. 2000;64:73–105.
13. Inga JR, Morsi BI. Effect of operating variables on the gas holdup in a large-scale slurry bubble column reactor operating with an organic liquid mixture. *Ind Eng Chem Res*. 1999;38:928–937.
14. Kim YH, Tsutsumi A, Yoshida K. Effect of particle size on gas holdup in three phase reactors. *Sàdhana*. 1987;10:261–268.
15. Jamialahmadi M, Mueller-Steinhagen H. Effect of solid particles on gas hold-up in bubble columns. *Can J Chem Eng*. 1991;69(1): 390–393.
16. Grevskott S, Sannaes BH, Dudukovic MP, Hjarbo KW, Svendsen HF. Liquid circulation, bubble size distributions and solids movement in two and three phase bubble columns. *Chem Eng Sci*. 1996;51(10):1703–1713.
17. Krishna R, De Swart JWA, Ellenberger J, Martina GB, Maretto C. Gas holdup in slurry bubble columns: effect of column diameter and slurry concentrations. *AIChE J*. 1997;43(2):311–316.
18. Chen P, Gupta P, Dudukovic, MP, Toseland BA. Hydrodynamics of slurry bubble column during dimethyl ether (DME) synthesis: gas–liquid recirculation model and radioactive tracer studies. *Chem Eng Sci*. 2006;61(19):6553–6570.
19. Warsito W, Fan LS. Measurement of real-time flow structures in gas–liquid and gas–liquid–solid flow systems using electrical capacitance tomography (ECT). *Chem Eng Sci*. 2001;56:6455–6462.
20. Soong Y, Blackwell AG, Harke FW, Ladner EP, Zarochak, MF. Ultrasonic characterizations of slurries in a bubble column reactor. *Ind Eng Chem Res*. 1999;38:2137–2143.
21. Cui Z, Fan LS, Turbulence energy distributions in bubbling gas–liquid and gas–liquid–solid flow systems. *Chem Eng Sci*. 2004;59(8–9):1755–1766.
22. Chilekar VP, Warnier MJF, van der Schaaf J, Kuster BFM, Schouten JC, van Ommen JR. Bubble size estimation in slurry bubble columns from pressure fluctuations. *AIChE J*. 2005;51(7):1924–1937.

23. Fischer F, Hoppe D, Schleicher E, Mattausch G, Flaske H, Bartel R, Hampel U. An ultra-fast electron beam X-ray tomography scanner. *Meas Sci Technol*. 2008;19:094002.
24. Tomiyama A. *Hybrid simulation of gas–liquid and gas–liquid–solid bubbly flows in bubble columns*. In: *10th Gas–Liquid and Gas–Liquid–Solid Reactor Engineering Congress*, Braga, Portugal, 2011.
25. Cassanello M, Larachi F, Guy C, Chaouki J. solids mixing in gas–liquid–solid fluidized beds: experiments and modeling. *Chem Eng Sci*. 1996;51(10):2011–2020.
26. Vandu CO, Koop K, Krishna R. Large bubble sizes and rise velocities in a bubble column slurry reactor. *Chem Eng Technol*. 2004;27(11):1195–1199.
27. Ruthiya KC, Chilekar VP, Warnier MJF, van der Schaaf J, Kuster BFM, Schouten JC, van Ommen JR. Detecting regime transitions in slurry bubble columns using pressure time series, *AIChE J*. 2005;51(7):1951–1965.
28. Kara S, Kelkar BG, Shah Y, Carr NL. Hydrodynamics and axial mixing in a three phase bubble column. *Ind Eng Chem Proc Des Dev*. 1982;21:584–594.
29. Sada E, Kumazawa H, Lee C, Iguchi T. Influence of suspended fine particles on gas holdup and mass transfer characteristics in a slurry bubble column. *AIChE J*. 1986;32:853–856.
30. Bukur DB, Daly JG, Patel SA, Application of gamma-ray attenuation for measurement of gas holdups and flow regime transitions in bubble columns. *Ind Eng Chem Res*. 1996;35(1):70–80.
31. Khare AS, Joshi JB. Effect of fine particles on gas holdup in three phase sparged reactors. *Chem Eng J*. 1990;44:11–25.
32. Mena PC, Ruzicka MC, Rocha FA, Teixeira JA, Drahos J. Effect of solids on homogeneous heterogeneous flow regime transition in bubble columns. *Chem Eng Sci*. 2005;60(22):6013–6026.
33. Reilly IG, Scott DS, de Bruijn TJW, Jain A, Piskorz J. A correlation for gas holdup in turbulent coalescing bubble column, *Can J Chem Eng*. 1986;64:705–717.
34. Sauer T, Hempel DC. Fluid dynamics and mass transfer in a bubble column with suspended particles. *Chem Eng Technol*. 1987;10: 180–189.
35. Koide K, Takazawa, A, Komura M, Matsunaga H. Gas holdup and volumetric liquid phase mass transfer coefficient in solid suspended bubble column. *J Chem Eng Jpn*. 1984;17:459–466.
36. Dudukovic MP. Opaque multiphase flows: experiments and modelling. *Expt Therm Fluid Sci*. 2002;26:747–761.
37. Chaouki J, Larachi F, Dudukovic MP. Non-invasive tomographic and velocimetric monitoring of multiphase flows. *Ind Eng Chem Res*. 1997;36:4476–4503.
38. Kumar SB, Moslemian D, Dudukovic MP. A γ-ray tomographic scanner for imaging voidage distribution in two phase flow system. *Flow Meas Instrum*. 1995;6(1):61–73.
39. Heindel TJ. A review of X-ray flow visualization with applications to multiphase flows. *J Fluids Eng*. 2011;133:074001-1–074001-5.
40. Marashdeh Q, Fan LS, Du B, Warsito W. Electrical capacitance Tomography—a perspective. *Ind Eng Chem Res*. 2008;47(10): 3708–3719.
41. Fischer F, Hampel U. Ultra-fast electron beam X-ray computed tomography for two-phase flow measurement. *Nucl Eng Des*. 2010;240(9):2254–2259.
42. Prasser H-M, Scholz D, Zippe C. Bubble size measurement using wire-mesh sensors. *Flow Meas Instrum*. 2001;12(4):299–312.
43. Joshi JB. Axial mixing in multiphase contactors: a unified correlation. *Trans Inst Chem Eng*. 1980;55:155–165.
44. Yianatos JB, Finch JA, Dobby OS, Xu M, Bubble size estimation in a bubble swarm. *J Colloid Interface Sci*. 1988;126(1):37–44.
45. Prasser H-M, Krepper E, Lucas. Evolution of the two phase flow in a vertical tube-decomposition of gas fraction profiles according to bubble size class using wire-mesh sensors. *Int J Therm Sci*. 2002;41:17–28.
46. Michelsen ML, Østergaard K. Holdup and mixing in gas liquid fluidized beds. *Chem Eng J*. 1970;1:37–46.
47. Ruzicka MC, Drahôs J, Mena PC, Teixeira JA. Effect of viscosity on homogeneous–heterogeneous flow regime transition in bubble column. *Chem Eng J*. 2003;96:15–22.

Manuscript received Mar. 13, 2012, revision received Jun. 18, 2012, and final revision received Aug. 30, 2012.